Groundwater for Sustainable Development 19 (2022) 100818

Contents lists available at ScienceDirect

Groundwater for Sustainable Development

journal homepage: www.elsevier.com/locate/gsd

Research paper

Hydrogeochemical and statistical approach to characterize groundwater salinity in the Ghiss-Nekkor coastal aquifers in the Al Hoceima province, Morocco

Yassine El Yousfi [a], Mahjoub Himi [a,b,*], Hossain El Ouarghi [a], Mohammed Elgettafi [c], Said Benyoussef [a,d], Hicham Gueddari [e], Mourad Aqnouy [f], Adil Salhi [g], Abdennabi Alitane [h]

[a] GEE, Laboratory of Applied Sciences (LSA), ENSAH Al Hoceima, Abdelmalek Essaadi University, Tetouan, Morocco
[b] MPGA, Faculty of Earth Science, University of Barcelona, Spain
[c] Mohamed First University (LCM2E-GES) Multidisciplinary Faculty of Nador, Selouane, Morocco
[d] Biology, Environment, and Health, Errachidia FST, University of Moulay Ismaïl, Meknes, Morocco
[e] OLMAN BPGE Laboratory, FPN (Nador), Mohamed First University, Oujda, Morocco
[f] AGRSRT, Applied Geology Research Laboratory, Errachidia FST, University Moulay Ismaïl, Meknes, Morocco
[g] Geography and Development Group, FLSH, Abdelmalek Essaadi University, Martil, Morocco
[h] WSEE, Laboratory of Geological Engineering, Faculty of Sciences, Moulay Ismail University, Meknes, Morocco

HIGHLIGHTS

- The bivariate correlation analysis shows a good relationship between TDS, EC, Cl, Na and Mg.
- The groundwater of Ghiss-Nekkor aquifer is mainly influenced by evaporation processes and missing with seawater.
- Geospatial analysis indicated significant spatial variation and heterogeneity in water quality measurements.
- Seawater intrusion is caused by normal faults along the plain to the west and east through which marine waters flow.

GRAPHICAL ABSTRACT

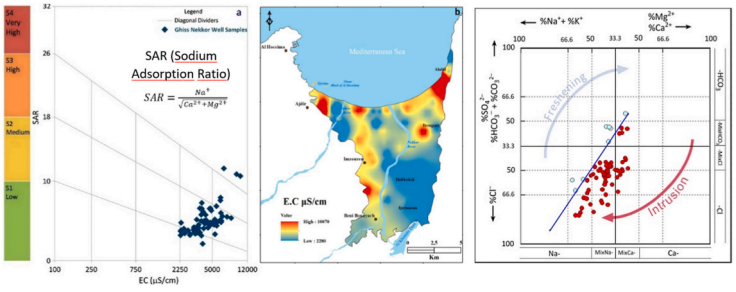

ARTICLE INFO

Keywords:
Hydrogeochemistry
Statistical analysis
Groundwater quality
Seawater intrusion
Ghiss-Nekkor aquifer

ABSTRACT

Seawater intrusion is one of the most severe problems confronting coastal aquifers. These aquifers are often considered significant freshwater sources, particularly in arid regions. The water resources mobilized at the Al Hoceima (Northeastern Morocco) come from the Ghiss-Nekkor aquifer and the Abdelkarim El Khattabi dam. The degradation of groundwater quality of the aquifer and the probability of marine intrusion has become a severe concern for the communities. The current study provides multidisciplinary research using hydrogeochemical and statistical approaches to evaluate groundwater quality and determine the origin of salinity in this aquifer. Depending on the direction of the water flow, he results indicate that most wells have a total salinity exceeding 2 g/L. The dominant chemical facies encountered are Na–Cl–Na–SO_4 resulting from rock-water interaction,

* Corresponding author. GEE, Laboratory of Applied Sciences (LSA), ENSAH Al Hoceima, Abdelmalek Essaadi University, Tetouan, Morocco.
E-mail address: himi@ub.edu (M. Himi).

https://doi.org/10.1016/j.gsd.2022.100818
Received 14 March 2022; Received in revised form 22 May 2022; Accepted 29 July 2022
Available online 7 August 2022

meaning that the breakdown of halite was the predominant source of groundwater mineralization. However, septic waste, water irrigation inflows, and locally seawater intrusion seem to substantially influence groundwater quality in this area.

1. Introduction

Groundwater is adopted as a strategic source of drinking water in semi-arid and arid climates. At least half of the world's population uses groundwater for drinking (Connor, 2015). About one-third of the world's population relies on groundwater to satisfy its daily requirements (Bieranye et al., 2016; UNESCO, 2012), and it is suspected that this is attributable to a decrease in the quality and availability of surface water resources (Beyene et al., 2019). Globally, approximately 2.1 billion people currently lack access to safe drinking water (WHO, 2017).

When aquifers hydraulically connected to the sea are subjected to excessive pumping, disequilibrium occurs, and the hydraulic gradient reverses. This causes seawater to move inland, producing what is known as seawater intrusion (Dunlop et al., 2019; Sato and Iwasa, 2011). The consequence is salinization of groundwater and deterioration of aquifer quality (Gaaloul and Cheng, 2003).

Seawater intrusion is the most severe environmental threat to Morocco's coastal aquifers (Benabdelouahab et al., 2018; Elmeknassi et al., 2021). The impacts of recent climate change on precipitation and temperature and vertical groundwater movements, affected by natural and anthropogenic processes, are leading the freshwater/seawater interface to advance and retreat (Kazakis et al., 2016).

The groundwater recharge and discharge balance determine the extent to which saltwater infiltrates, the piezometric level of the aquifer, the distance from the aquifer to the saltwater sources and its geological structure (Kumar, 2015).

Salinization of coastal aquifers may be attributed to direct saltwater intrusion or to a variety of complicated geochemical processes that affect water quality in a variety of ways, including water-rock interactions, brine mobilization, and anthropogenic pollution (Mondal et al., 2010). In this context, it is critical to understand the chemical mechanisms behind the salinization of coastal aquifers to manage these vulnerable water resources in the future.

Morocco's groundwater salinization has been intensively investigated in the last years (Elgettafi et al., 2013; Elmeknassi et al., 2021; Himi et al., 2017). Understanding the source of groundwater salinity is critical for effective aquifer management. (Kamal et al., 2021; Rochdane et al., 2022). Groundwater's chemical composition is strongly altered by the liquid phase and the solid matrix interactions. (Mahlknecht et al., 2017). Chemical interactions have been studied using hydrogeochemistry approaches such as minor, major, and trace elements, ionic ratios, ionic deltas, mixing calculations, and geochemical modelling (Liu et al., 2017). Geochemical analyses of groundwater can provide valuable information and explain possible areas of salinization, their source and related geochemical processes in the saltwater/freshwater transition zone (Panteleit et al., 2001). The HFE-Graphic developed by Giménez-Forcada (2010) is a diagram that explains the hydrochemistry of intrusion and recovery of marine intrusion-related processes in an aquifer system. However, it may be substituted by other hydrochemical diagrams, such as the Piper diagram. Multivariate data analysis is used to categorize variables and observable units and define their relationship. The procedures for classification are non-hierarchical and hierarchical clusters analysis and discriminant analysis. Several techniques

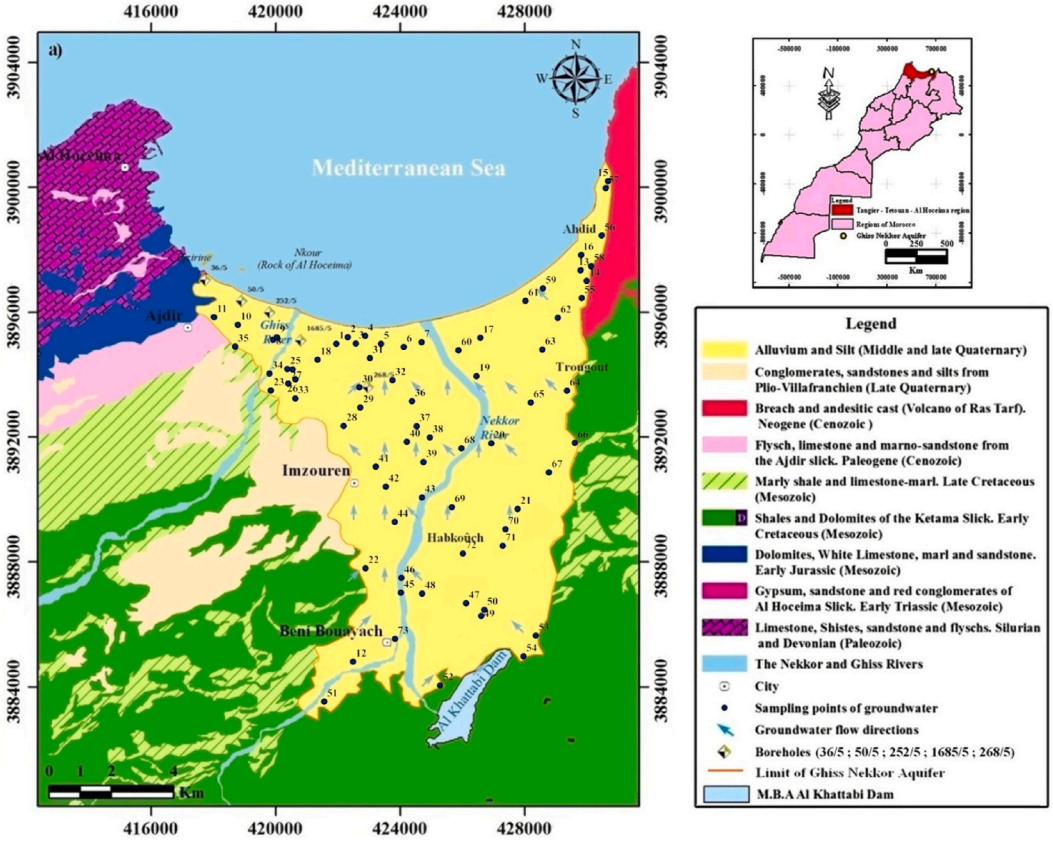

Fig. 1. Location map of the Ghiss-Nekkor aquifer and simplified geological map of the studied area showing sampling points with groundwater flow directions.

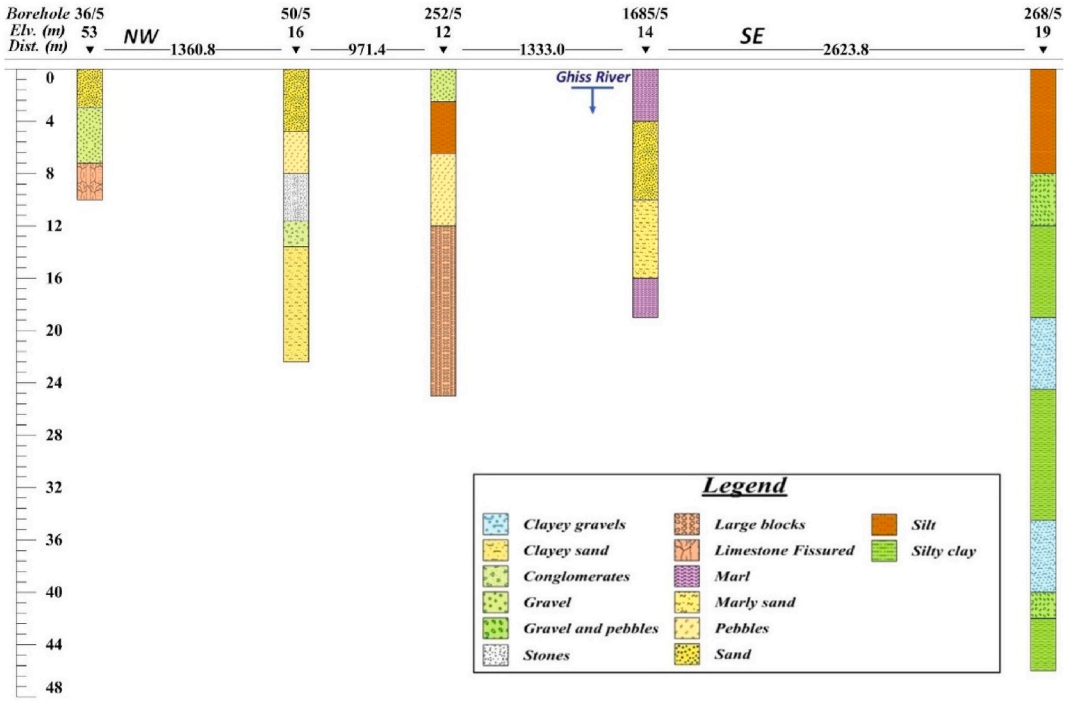

Fig. 2. Simplified geological cross-section in the Ghiss-Nekkor aquifer.

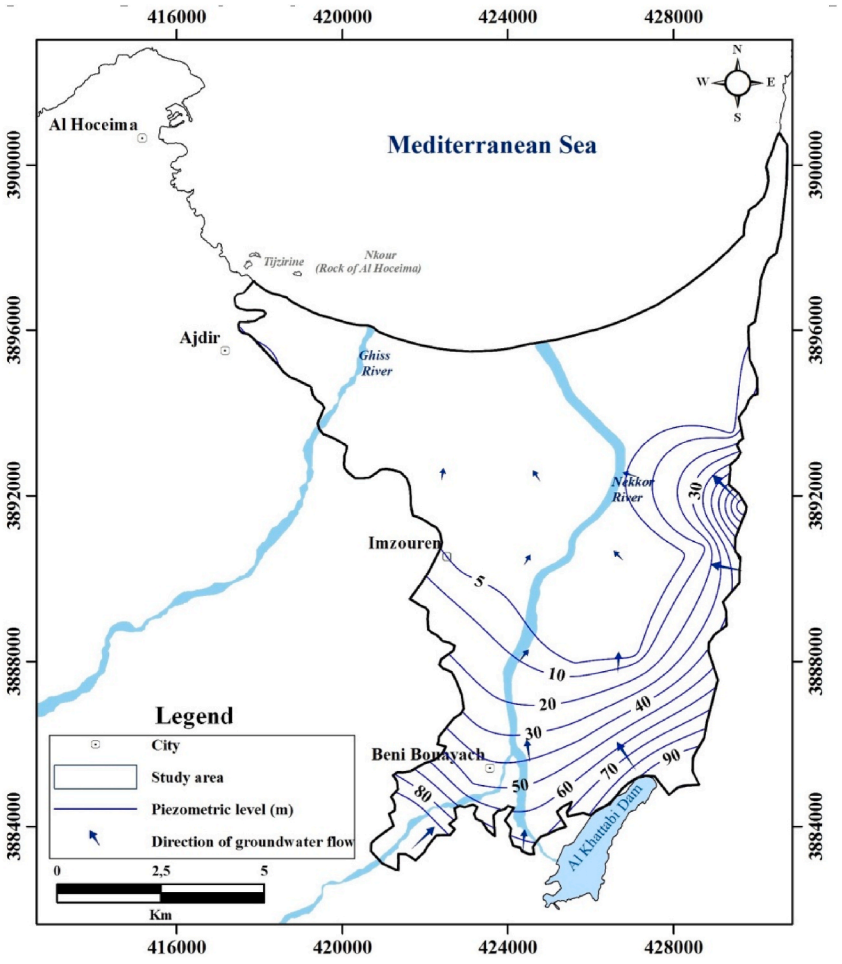

Fig. 3. Piezometric map of the Ghiss Nekkor auqifer (January 2018).

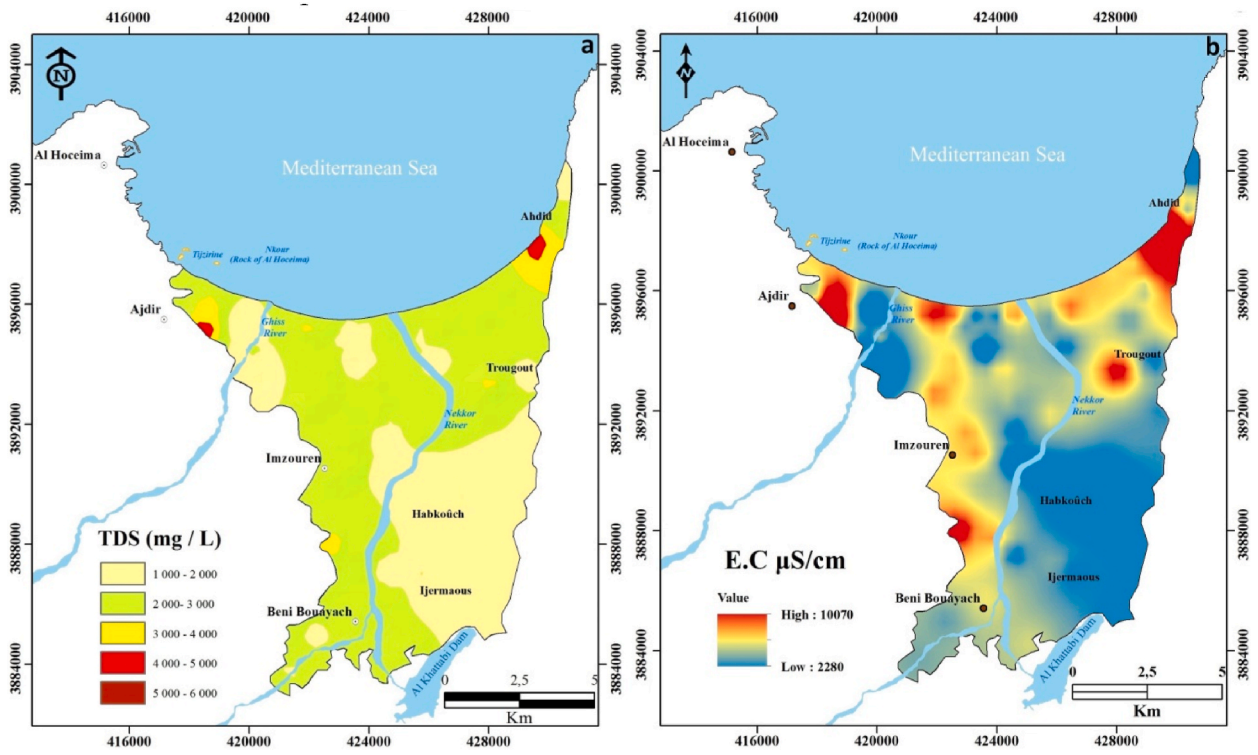

Fig. 4. Spatial distribution of TDS (a) and electrical conductivity (b) in the Ghiss-Nekkor aquifer.

quantify those statistical parameters that distinguish groups from previous data. Integrated research of hydrogeochemical and statistical analytic methodologies was carried out to understand the source of groundwater salinity and the causes of pollution in the Ghiss-Nekkor aquifer. It is common practice to utilize chemical elements and statistical analysis to determine the complex contribution of many different sources to a simple combination of them. The relationships between major ions and Cl/Br ratio are very dependable and widely used methodologies for assessing the source of salinity and contaminants.

2. Geological and hydrogeological setting

The Ghiss-Nekkor aquifer is located in Al Hoceima province, northeast of Morocco. It is a coastal plain covering an area of 100 km^2, drained and crossed by two rivers: Nekkor River in the centre of the site (From South to North) and Ghiss River in the Ouest part (Fig. 1). From a geological perspective, the study area is a Plio-Quaternary alluvial deposit, with a predominance of detrital sediments, mainly gravel, sand, silt, and clay, resting on a bedrock formed by blue shales, marls and primary quartzites, and silts of middle and ancient quaternary age. In the east and southwest, we find a series of grey or black sericite schists with quartzite banks of the Albo-Aptian and the simultaneous presence of dolomites. In addition, volcanic formations are arranged in an andesitic flow. To the north of the plain, we find successively in the west flysch, a series of marl-sandstone and microbrecciated limestone banks of Eocene of the nappe of Ajdir.

To have a better understanding of the lithological complexity of the aquifer, we represent the lithological logs of some boreholes (36/5, 50/5, 252/5, 1685/5, and 268), which shows a variety of facies (Fig. 2), towards the centre, we find a more critical dominance of sands, silts, silty clays, gravels and marls, marly sands along the Ghiss River. As well as, to the west, we note the dominance of carbonate formations, which is the dorsal limestone massif of Bokkoya. Indeed, the informations in the centre bevel laterally and generally influence the geometry of the reservoir, thus giving rise to the presence of water tables within marly lenses.

A primary piezometric survey was conducted in 2018 for this investigation (Fig. 3). The total piezometric survey included 73 wells. Each piezometric study was carried out over a week to ensure comparable groundwater levels. The sampling point's data altitudes (land surface elevations) were derived using ArcGIS software from a Digital Elevation Model. A system of aquifers containing a free water table, flows mainly SE-NW toward the Mediterranean Sea. In the southeast part, the hydraulic gradient is relatively elevated. It is high in the upstream section (7.3%) and defined by relatively narrow piezometric lines but low in the downstream part (0.8%). It is characterized by dispersed piezometric lines in the northwest area close to the sea. The variance in piezometric levels is influenced by several causes, including less rainfall due to the drought period and overuse of water resources. Moving towards the sea, we note the presence of the 0 m isopiez inland (Fig. 3) which reflects the contribution of marine intrusion in the salinization of the groundwater aquifer. A system of aquifers containing a free water table flows mainly SE-NW toward the Mediterranean Sea. In the southeast part, the hydraulic gradient is relatively elevated. It is high in the upstream section (7.3%) and defined by relatively narrow piezometric lines, but low in the downstream part (0.8%) and characterized by dispersed piezometric lines in the northwest area close to the sea. The variance in piezometric levels is influenced by several causes, including less rainfall due to the drought period and overuse of water resources. Moving towards the sea, we note the presence of the 0 m isopiez inland (Fig. 3) which reflects the contribution of marine intrusion in the salinization of the groundwater aquifer.

3. Materials and methods

3.1. Sampling and laboratory analysis

Seventy-three samples were collected during field missions in May 2018 to characterize groundwater's hydrogeochemistry. Temperature (T), pH, Total Dissolved Solids (TDS) and electrical conductivity (EC) were measured in situ immediately after sampling using the multiparameter device (HANA HI 98194), which has an accuracy of ±0.01 units

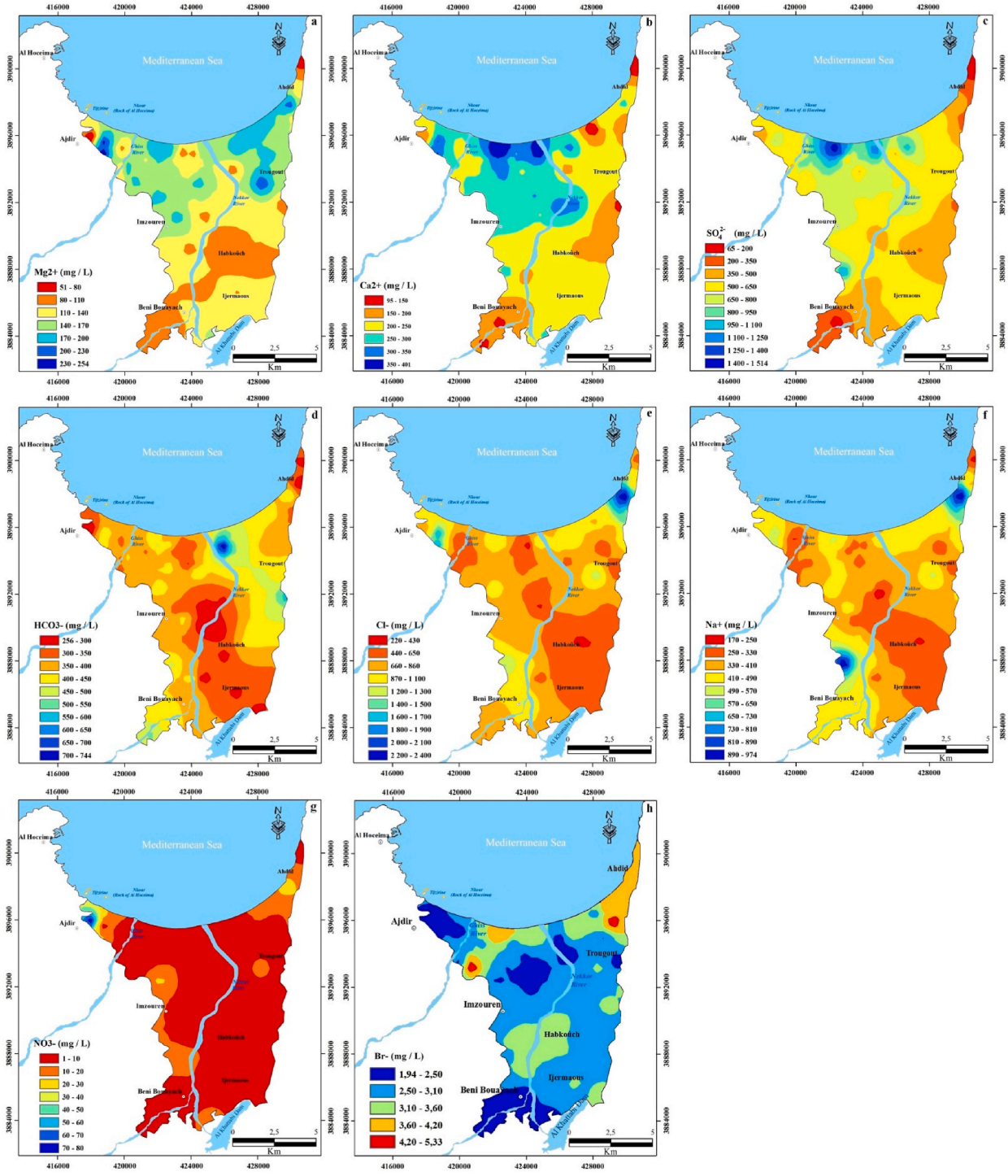

Fig. 5. Spatial variability of major element concentrations in groundwater of the Ghiss-Nekkor aquifer. (a) Magnesium Mg^{2+}, (b) Calcium Ca^{2+}, (c) Sulfate SO_4^{2-}, (d) Bicarbonate HCO_3^-, (e) Chloride Cl^-, (f) Sodium Na^+, (g) Nitrate NO_3^-, (h) Bromide Br^-.

for pH and ±1% (or ±1 μS/cm) for electrical conductivity. The samples are taken in the field in two bottles after filtration at ($\varphi = 0.45$ μm), one for the anions and the other for the acidified cations. For wells equipped with a pump, samples are taken after pumping.

The analyses cover 13 parameters; these are pH, T, TDS, EC, Na^+, Mg^{2+}, K^+, Cl^-, Ca^{2+}, Br^-, SO_4^{2-}, HCO_3^- and NO_3^-. The measurements of cations (Na^+, Mg^{2+}, K^+, and Ca^{2+}), and anions (Cl^-, HCO_3^-, SO_4^{2-}, Br^- and NO_3^-) of the sampled waters were carried out using the spectrophotometer Shimadzu UV-1800, Flame Photometer CL 361, HACH LANGE DR 1900 at the laboratory LSA-GE2 of ENSA Al Hoceima, except that for the concentrations of bromides which were carried out in the technical and scientific services of the University of Barcelona. The statistical analyses were performed under the software Python 3.8 and XLSTAT. The parameter values were compared to those established by the WHO. The ionic charge balance error for the obtained result was between 5% and 10% for all samples, which is an acceptable error for this study and shows the chemical analysis accuracy.

3.2. Statistical analysis

The study and determination of the relationships between chemical elements and their graphical representation revealed that many of physicochemical and chemical parameters were relevant when considered separately (Hamzaoui-Azaza et al., 2011). Most of the time, there is one (or more) relationship between these factors that explain the evolution of groundwater chemistry. As a result, it was interesting to put the data through a statistical procedure using a multivariate statistical technique set of core component analysis (PCA). These approaches can be used with graphical depictions to improve the interpretation of hydrochemical parameters. The PCA was performed using all hydrochemical data, including important cations and anions. As well as PCA condenses the information into numerous variables through a set of linear weighted combinations of all those variables, which makes no distinction between common and unique variants (Kim and Lee, 2017). The intermediate correlation matrices and variable projection in the F1 and F2 axes space were generated using the Python 3.8 program. The hydrochemical approach involved the application of a "Piper diagram" under the software diagrams for the classification of waters according to their hydrochemical composition. GIS tools are necessary when it comes to manipulating and processing diverse and meaningful spatial data, as they offer excellent possibilities for the spatial variation of parameters (Alitane et al., 2022; Mohajane et al., 2021).

4. Results and discussion

4.1. Characteristics of groundwater and its hydrochemistry

The TDS (total dissolved solids) shows a substantial spatial difference varying between 1130 mg/L and 5035 mg/L with an average value of 2222 mg/L. Based on the TDS classification of Robinove et al. (1958). The saline waters are classified into four groups of freshwater. Overall, the Ghiss-Nekkor samples are highly mineralized (between 1000 and 5035 mg/L). The spatial distribution (Fig. 4a) of TDS shows the increase of the saline load towards the outlets (Sea, Ghiss and Nekkor Rivers) with concentrations above 2500 mg/L. The highest TDS values were recorded mainly in the North (Ait Youssef Ou Ali and Ahdid).

Electrical conductivity (EC) is a good indicator for determining the degree of overall mineralization of water. Electrical conductivity obtained from this analysis are included between 2280 µS/cm and 10,070 µS/cm with an average of 4433 µS/cm ± 0,4 µs/cm (Fig. 4b). Thus, its values indicate a significant variation in the chemical components of the water; the lowest value corresponds to well N°9 (2280), while the highest value has been recorded in the well N°16 (10,070). According to the standards recommended by the WHO (2011) for the assessment of overall groundwater quality where the electrical conductivity of groundwater should not exceed 2700 µS/cm. Generally, the electrical conductivity is beyond the threshold of the standards defined by WHO; only about 8.22% of the samples meet these standards. The remaining 91.78% have conductivity between 2747 and 10,070 µS/cm, indicating mineralized waters and are unfit for human consumption.

The hydrogen potential (pH) and temperature values of the studied well water are in the normal range of the World Health Organization (WHO, 2011) guidelines. More than 79% of the water in the Ghiss-Nekkor aquifer has a pH above 7. They vary between 6.6 and 8.0 for pH and 18.1 °C and 25.4 °C for temperature. Therefore, the proof is made that these waters studied come from shallower aquifers for the most part.

Magnesium contents range from 53.8 to 254.4 mg/L (Fig. 5a), the highest concentrations are observed in areas such as Ait Youssef Ou Ali, Azrar, Trougout, and Sfiha. The calcium element (Ca^{2+}) at concentrations vary between 94.6 and 400.8 mg/L (Fig. 5b) with very low values

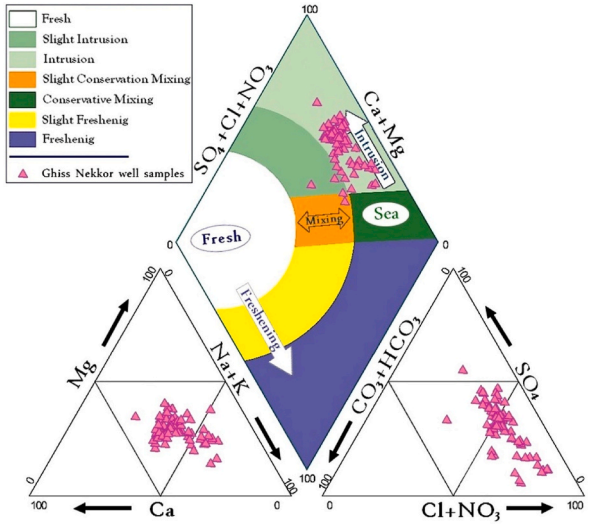

Fig. 6. Hydrochemical classification of groundwater from wells in the Ghiss-Nekkor aquifer by Piper diagram (Piper, 1944).

from South-West (Beni Bouayach) to North-East (Azrar) and higher values in the North-West (Imzouren) to North (Ait Youssef Ou Ali). Significant levels in Trougout, Ijermaous, and Ajdir are also observed.

Sulfates (Fig. 5c) in the groundwater have a content ranging from 64.6 mg/L (Ahdid, Azrar) and 1514.3 mg/L (Soauni, Ait Youssef Ou Ali). There is an extreme increase in the contents in the North and South-West; they are very concentrated around the bay of Al Hoceima. The average frequency of Bicarbonate element HCO_3^- is 381,7 mg/L with the maximum amount of 744,2 mg/L (Fig.5d) and a minimum of 256,2 mg/L.

Cl^- ion concentrations vary from 213 mg/L (Trougout) to 2698 mg/L (Azrar) (Fig. 5e). They do not comply with WHO standards (200 mg/L). Mapping of this component indicates the highest concentration in the North-East and North-West parts of the valleys up to the summits. Low concentrations are recorded in the south-eastern part, increasing progressively towards the north-eastern and north-western parts.

The values of Na^+ ion concentrations vary from 170 mg/L (Ait Youssef Ou Ali) to 954 mg/L (Azrar) (Fig. 5f). With an average value of 381.7 mg/L. Potassium (K^+) concentration ranged from 1.4 to 45.3 mg/L, with an average value of 6.3 mg/L. The highest allowed value of K^+ in groundwater is 12.0 mg/L (milligrams per liter of water) (Standard, 1997), and 87.67% of the samples were within the allowable limit. It is present in trace amounts with variations of 1.4 mg/L (Tanouthouzag, Oued Nekkor River) and 45.3 mg/L (Sfiha, Ait Youssef Ou Ali) and (Rhach, Azrar). Bromide levels (Fig. 5h) generally increase from upstream to the ocean.

4.2. Groundwater hydrochemical facies evolution

The hydrochemical facies describe groundwater bodies in an aquifer that differ in geochemical characteristics (Yang et al., 2016).

The hydrochemical facies of the Ghiss-Nekkor aquifer is given in Fig. 6. For this investigation, a modified Piper diagram (Kelly, 2005) was used from the analysis of this diagram. We observe two types of chemical facies: chloride and sulfate calcic and magnesic and chloride sodium or sulfate sodium with a tendency to the chloride and sulfate poles for the anions subtriangle and a tendency towards the calcium and magnesium poles for the cations subtriangle. The waters of some local wells tend different facies, chloride calcic for the waters of Azrar and Beni Bouayach. However, the sulfated calcic facies exist and is observed in the water points of Ait Youssef Ou Ali.

Table 1
Results of physicochemical analysis of groundwater of the Ghiss-Nekkor Aquifer.

Wells	pH	T(°C)	EC	TDS	Na^+	K^+	Mg^{2+}	Ca^{2+}	Cl^-	NO_3^-	HCO_3^-	SO_4^{2-}	Br^-	Cl^-/Br^-	Ionic balance
			(μS/cm)	(mg/L)	mg/L)	(mg/L)	(mg/L)	mg/L)	(mg/L)	(mg/L)	(mg/L)	(mg/L)	(mg/L)		(%)
1	7,5	19,5	6310	3155	470,5	5,3	199,7	343,1	1065	2,1	478,9	1311,7	4,1	259,8	−9
2	7,4	18,3	6110	3055	485	6,5	194,2	376,1	1029,5	3,4	386	1514	4,1	251,1	−9
3	7,1	18,1	6244	3122	470,5	7,4	201,6	384,8	1047,3	9	466,7	1479,9	4,1	255,4	−9
4	7,3	19,4	5244	2622	414,5	4,1	176,6	349,5	869,7	11,4	378,2	1166,4	4,1	212,1	−5
5	7,4	19,5	3303	1652	281	6,3	82,6	275,8	461,5	7,1	326,4	718,9	3,1	148,9	−1
6	7,3	20,1	3514	1757	292,5	3,8	97,9	285,4	266,2	6,4	335,5	772,5	3,5	76,1	9
7	7,4	20,3	5601	2800	417,5	4,3	172,8	400,8	1100,5	2,9	381,3	1242,8	3,4	323,7	−9
8	8,0	19,3	2901	1130	236,5	3,3	86,4	240,5	426	2,4	298,9	543	2,4	177,5	2
9	7,8	18,9	2280	1140	236	3	126,7	208,4	568	9,7	414,8	458,9	2,4	236,7	−2
10	7,4	19,5	7218	3609	536	13,7	232,3	333,5	1668,5	5,5	445,3	799,2	2,4	695,2	−9
11	8,0	20,3	3869	1934	401,5	45,3	50,8	143,5	710	79,9	260,2	349,9	2,5	284,0	−5
12	7,5	20,4	3880	1935	396,5	2,5	85,4	139,5	781	8,7	427	151,1	1,9	411,1	−2
13	7,7	21,0	9166	4581	886	17,2	187,6	210,4	2272	18,5	405,7	432,1	3,7	614,1	−10
14	7,7	20,0	6156	3065	564,5	13,5	127	160,3	1455,5	11,7	332,5	279,5	3,7	393,4	−10
15	7,8	21.7	2310	1155	260,5	10,7	61,4	125,1	639	4,1	326,4	64,6	3,7	172,2	−4
16	7,8	20,8	10,070	5035	974	29,1	227,4	270,1	2598	33,8	471,9	506,3	3,7	702,2	−10
17	7,7	25,4	5695	2847	438,5	9,5	190,1	307,8	1065	3,4	469,7	1001,9	3,6	295,8	−8
18	7,7	19,3	4298	2149	385,5	9,2	131,5	216,4	674,5	2,2	340,4	860,4	2,8	240,9	−5
19	7,6	23,2	3414	1707	338	1,4	97	165,1	568	3,1	445,3	501	2,2	258,2	−4
20	7,6	20,8	4538	2269	379,5	3	111,4	304,6	852	8,3	397,7	753,4	3,1	274,8	−6
21	7,3	21,5	3180	1590	298	1,7	115,2	192,4	639	8,6	433,1	439,8	2,8	228,2	−4
22	7,4	20,8	6687	3344	896	4,8	121	253,3	1349	12,9	463,6	1040,2	3	449,7	−5
23	7,4	21,5	3178	1593	270	4	120	184,4	568	3,9	341,6	546,8	2,4	236,7	−3
24	7,0	19,6	3386	1933	334	1,7	158,4	224,5	497	3,8	378,2	833,7	3	165,7	2
25	7,0	20,3	4521	2259	357	1,7	201,6	232,5	639	9,9	457,5	1021	2,4	266,3	−4
26	7,0	18,9	3280	1637	262,5	3,3	144	208,4	603,5	4,3	384,3	520,1	4,3	140,3	−1
27	7,0	20,0	2747	1674	331	2,8	201,6	240,5	603,5	3,2	390,4	718,9	2,8	215,5	6
28	6,6	20,9	5594	2802	423,5	8,9	172,8	272,5	994	23,7	420,9	661,6	2,4	414,2	−3
29	7,0	24,3	5159	2602	408,5	3,9	163,2	280,6	816,5	10,8	396,5	699,8	2,5	326,6	1
30	6,7	20,9	5049	2524	411,5	3,8	163,2	288,6	816,5	9,6	420,9	703,6	2,6	314,0	1
31	7,1	18,9	3693	1845	279	2,9	124,8	264,5	603,5	2,5	311,1	485,7	2,6	232,1	5
32	7,2	20,5	2305	1260	278	2,9	119,6	222,5	461,5	4,8	305	462,7	2,3	200,7	9
33	7,0	19,5	2475	1224	341,5	7,5	172,8	264,5	852	9,2	384,3	481,8	5,3	160,8	2
34	7,0	21,0	3284	1699	262,5	3,8	120	256,5	497	5,9	341,6	393,9	2,4	207,1	10
35	7,0	19,7	8037	4019	535,5	10,5	254,4	336,7	1775	21,2	427	546,8	2,5	710,0	−6
36	7,0	19,9	4960	2470	400	3,6	187,2	264,5	710	6,8	463,6	776,3	2,3	308,7	2
37	7,0	19,9	4528	2251	354,5	3,5	158,4	288,6	639	4,9	341,6	699,8	2,3	277,8	6
38	7,1	20,6	3950	1973	170	1,5	134,4	272,5	568	5,8	317,2	569,8	2,6	218,5	−2
39	7,0	19,8	3256	1632	247,5	2,8	96	232,5	355	5,9	256,2	497,1	2,7	131,5	10
40	7,4	19,8	4061	2033	320	3,8	124,8	272,5	568	6,7	347,7	600,4	2,3	247,0	5
41	7,0	21,4	5337	2669	443	9,1	182,4	256,5	852	9,1	340,1	734,2	2,8	304,3	2
42	7,0	24,5	5363	2681	267,5	3,4	153,6	240,5	852	10,2	430,1	623,3	3,1	274,8	−10
43	7,4	21,2	2881	1441	234,5	3	115,2	216,4	745,5	6,6	256,2	358,6	3,1	240,5	−4
44	7,6	20,7	4249	2124	400	4,6	105,6	192,4	674,5	7,9	353,8	546,8	3,2	210,8	−1
45	7,1	20,7	4807	2403	440,5	4,3	86,4	200,4	958,5	11,2	439,2	342,6	3,4	281,9	−7
46	8,0	20,9	5546	2773	500,5	5	148,8	160,3	1065	15,3	366	550,7	3,6	295.8	−6
47	7,0	22,3	4100	2048	374	2,4	124,8	216,4	639	5	353,8	631	2,5	255,6	0
48	7,4	23,4	3235	1618	259	3,2	96	240,5	497	3,6	268,4	455,1	2,9	171,4	6
49	8,0	20,4	3512	1756	318	4	134,4	208,4	568	4,2	280,6	543	3,2	177,5	5
50	7,2	21,1	3538	1770	257,5	2,2	105,6	232,5	568	4,4	329,4	489,5	3,1	183,2	0
51	7,5	20,3	3982	1991	390	2,7	96	144,3	639	4,7	500,2	271,1	2,1	304,3	0
52	7,3	23,0	4530	2366	386	6,5	148,8	248,5	852	14,4	372,1	493,3	2,1	405,7	1
53	7,0	24,1	3580	1796	309,5	4	115,2	240,5	532,5	4,6	311,1	504,8	3,1	171,8	7
54	7,0	20,6	3540	1771	307	4,5	129,6	216,4	568	1,9	305	516,3	3,2	177,5	5
55	7,2	22,4	6124	3034	533,5	14,3	134,8	158,3	1349	10,8	347,7	322	4,2	321,2	−9
56	7,7	20,9	4148	2065	339	14	117,6	204,4	852	13,8	262,3	274,6	3,7	230,3	1
57	7,2	22,4	2286	1166	218,5	12,1	86,4	124,3	568	3,9	292,8	69,6	3,7	153,5	2
58	7,2	20,9	6216	3108	469,5	6,2	142	210,4	1455,5	18,1	352,1	258,9	3,7	393,4	−10
59	7,3	21,1	4774	2393	399	16,6	175,2	240,5	887,5	13	460,6	611,9	3,9	227,6	−1
60	7,0	25,1	3811	1906	442	9	141,6	212,4	923	3,1	744,2	443,6	2,1	439,5	−7
61	7,5	25,0	4898	2449	452,5	9,1	181	94,6	816,5	10,7	424	634,8	2,8	291,6	−5
62	7,2	25,2	4236	2118	363	7,2	156	200	639	4,7	366	501	4,7	136,0	6
63	7,4	25,3	3836	1918	251,5	3	172,8	200	461,5	5,8	359,9	600,4	2,5	184,6	6
64	7,0	24,6	3417	1708	272	3,9	153,6	204,4	426	5,8	405,7	642,5	2,2	193,6	4
65	7,5	21,6	6466	3177	490	4,4	220,8	220,4	1242,5	13,9	460,6	631	3,2	388,3	−5
66	7,5	23,3	3679	1840	396,5	2,9	86,4	132,3	674,5	0,9	555,1	281,8	3,1	217,6	−5
67	7,8	22,0	3818	1910	353	4,4	139,2	152,3	603,5	7,6	463,6	451,2	3,2	188,6	1
68	7,5	20,6	4744	2372	378	2,6	136,8	316,6	816,5	5	298,9	722,8	3	272,2	1
69	7,3	20,6	3153	1574	272,5	3,2	91,2	208,4	426	5,3	286,7	501	3,4	125,3	5
70	7,1	20,6	2530	1265	211,5	2,1	84,8	150,3	213	5,5	436,2	314,3	2,9	73,4	9
71	7,3	20,6	3575	1788	322	2,5	110,4	204,4	603,5	7,2	375,2	489,5	3	201,2	0
72	7,2	20,6	3575	1788	302	3,7	110,4	224,5	532,5	2,7	295,9	588,9	3,1	171,8	2
73	7,0	22,8	4697	2342	463	3,4	120,4	166,3	1136	6,7	401,8	366,4	2,1	541,0	−9

Table 2
Pearson correlation matrix for Ghiss-Nekkor aquifer parameters.

	pH	T(°C)	EC	TDS	Na^+	K^+	Mg^{2+}	Ca^{2+}	Cl^-	NO_3^-	HCO_3^-	SO_4^{2-}	Br^-
pH	1.00												
T(°C)	−0.07	1.00											
EC	0.09	−0.05	1.00										
TDS	0.06	−0.05	1.00	1.00									
Na^+	0.20	−0.04	0.87	0.88	1.00								
K^+	0.35	−0.02	0.40	0.40	0.46	1.00							
Mg^{2+}	−0.21	−0.04	0.66	0.68	0.47	0.09	1.00						
Ca^{2+}	−0.25	−0.36	0.39	0.39	0.16	−0.10	0.54	1.00					
Cl^-	0.17	−0.06	0.91	0.91	0.89	0.50	0.57	0.23	1.00				
NO_3^-	0.23	−0.07	0.33	0.33	0.37	0.82	0.02	−0.10	0.37	1.00			
HCO_3^-	−0.11	0.22	0.33	0.33	0.39	−0.03	0.38	0.04	0.32	−0.06	1.00		
SO_4^{2-}	−0.11	−0.26	0.35	0.36	0.22	−0.14	0.56	0.78	0.10	−0.13	0.19	1.00	
Br^-	0.13	−0.13	0.20	0.19	0.20	0.20	0.16	0.14	0.25	−0.01	−0.10	0.17	1.00

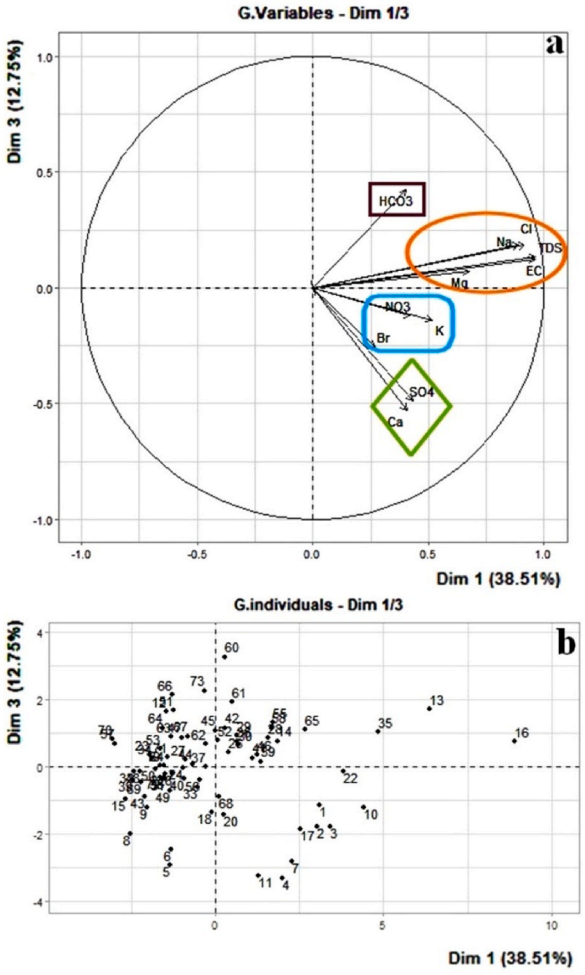

Fig. 7. (a) Variable projection on the F1–F2 plane using Principal Component Analysis. (b) The chemical composition of groundwater from Ghiss-Nekkor was used to generate a principal component analysis plot.

The values generated from the analysis of groundwater samples from the Ghiss-Nekkor aquifer and plotted on Piper's diagram reveal that the loss of sodium could be accounted by the cation exchange process and by carbonates equilibrium, as are the elevated Ca^{2+} concentrations and decrease in Na^+ levels explained by the retention of Na^+ by exchange with Ca^{2+} and Mg^{2+} (see Table 1).

4.3. Statistical analysis

4.3.1. Correlation analysis

Since the correlation factor is applied as a preliminary assessment of the hydrochemical source of the facies and to make suggestions of possible geochemical processes that may be controlling the origin of water chemistry, establishing the significant source of salinity based on TDS and EC, a bivariate correlation technique is initially applied, assuming that a correlation factor R2 >0.5 implies a statistically significant degree of correlation. EC and TDS show a good correlation with Cl^-, Na^+ and Mg^{2+} (Table 2), suggesting that these elements are the principal sources of mineralization. There was also a good and positive correlation between Cl^- and Na^+, and Cl^- and Mg^{2+} demonstrating that these elements could be originated from seawater and weathering of chloride minerals (NaCl, MgCl). SO_4^{2-} is significantly correlated with Ca^{2+} and Mg^{2+} ($R^2 = 0.78$ and 0.56 respectively), suggesting that they probably have an evaporite origin ($CaMgSO_4$). In addition, NO_3^- shows a strong correlation with K^+ ($R^2 = 0.82$), suggesting an anthropogenic source of these ions. No relationship was found between Ca^{2+}, Mg^{2+} and HCO_3^-, indicating that carbonate alteration did not significantly regulate the origin of sulfate in the groundwater under investigation.

4.3.2. Principal component analysis (PCA)

To determine the most significant elements affecting groundwater chemistry, a principal component analysis (PCA) was done. Eleven hydrochemical variables were considered: EC, TDS, Mg^{2+}, Ca^{2+}, K^+, Na^+, SO_4-, Br^-, Cl^-, HCO_3^-, and NO_3. Two factors (F1 and F2) allowed us to reinforce the perceived tendencies and to classify the variables into four distinct groups (Fig. 7a), Na^+, Cl^-, Mg^{2+}, EC, and total dissolved solids (TDS) comprise the first correlation group, NO_3^- and K^+ the second group and Ca^{2+} and SO_4^{2-} make up the third group. HCO_3^- make alone the fourth group. The horizontal axis is used to plot PC 1, and the vertical axis is used to plot PC 2 (Fig. 7b). This proportion is modest, implying that the variance is only somewhat structured. This is because the chemistry of water is influenced by various variables (Trabelsi et al., 2012). The first component (PC1) entered at 38.51% of the variance is highly related to the EC, TDS, Mg^{2+}, Cl^- and Na^+. Which explains the dissolution of sedimentary and evaporate rocks that are present in the Ghiss-Nekkor aquifer (Benyoussef et al., 2021) or seawater intrusion. As a reason, this component represents the signature indication of the water-rock interaction process. The second component (PC2), which contains in majority SO_4^{2-} and Ca^{2+}, explains 12.75% of the variation and indicates gypsum dissolution. Anthropogenic activities and their effects on the Ghiss-Nekkor aquifer is mainly related to the NO_3^- and K^+ chemical fertilizers.

4.4. Groundwater salinization processes

4.4.1. Gibbs diagram

Gibbs R. J., (1970) describes five mechanisms (precipitation

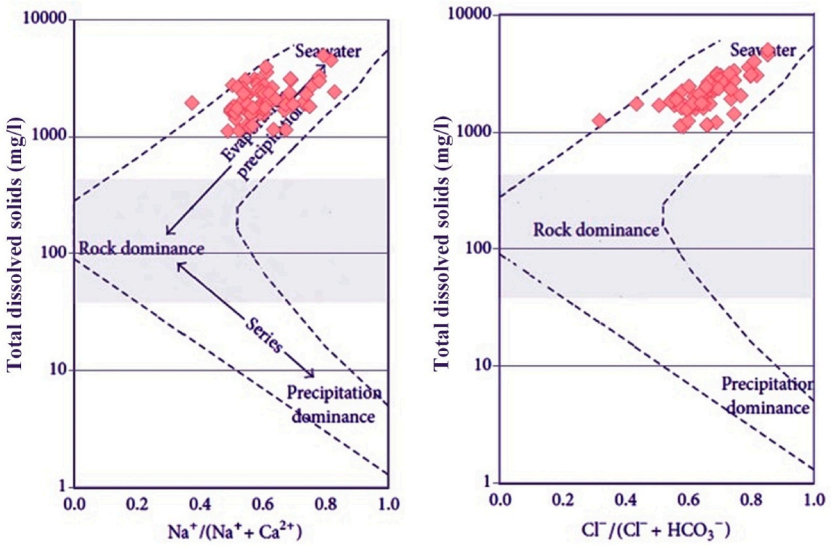

Fig. 8. Gibbs diagram for the Ghiss-Nekkor aquifer.

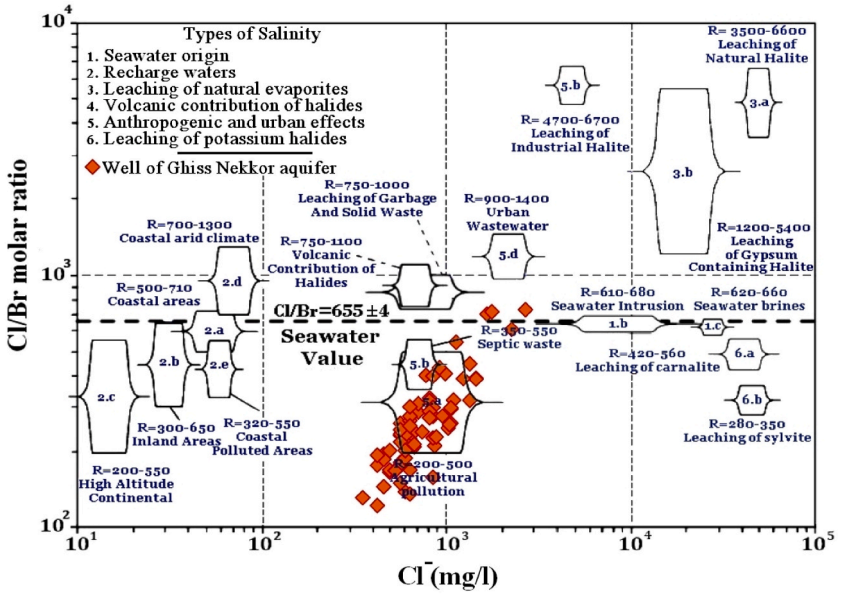

Fig. 9. Linear regression between Cl^- concentration and Cl/Br ratio of groundwater samples in the research area Projected in data from (Alcalá and Custodio, 2008).

dominance, evaporation, rock dominance, precipitation, and mixing) that control the overall groundwater chemistry (Fig. 8). The majority of the Groundwater samples are near seawater and are plotted graphically in the upper right corner of the Gibbs diagram, indicating that groundwater of Ghiss-Nekkor is mainly influenced by evaporation processes and mixing with seawater.

To highlight and define the processes involved in groundwater salinization, various chemical correlations were established (Fig. 9) illustrate a correlation between Cl^-/Br^- and Cl^-, Chloride and bromide ions are assumed to be conservative groundwater components since they do not interact in ion-exchange or redox reactions and do not produce an insoluble precipitate (Daniele et al., 2011; Davis et al., 1998). Chloride shows high concentrations in the wells (35, 13, and 16) is generally near the coastal fringe. The salinity of these samples is probably attributed to seawater intrusion. This growth is associated with the dissolution of marine aerosols rich in chloride. Aquifer saltwater intrusion may be caused by deep faults cutting through impermeable layers of clays and silts or by lateral facies alteration in shallow deposits, which might explain the occurrence of saltwater. A high Cl^-/Br^- ratio is almost always considered a good predictor of domestic water impact. (Vengosh and Pankratov, 1998). The existence of polluted discharges without prior treatment (agricultural products and wastewater) can also explain the high chloride concentration in areas far from the threat of maritime intrusion. The samples collected in the Ghiss-Nekkor plain indicate Cl/Br variations in the range of 73.4–710, with an average value of 273.1. Most samples are distributed between agricultural pollution and septic waste, with a tendency to leach evaporate rocks (Fig. 9). Cl^-/Br^- ratios enabled the identification of two major sources of human-induced pollution: (i) septic effluents, particularly in urban zones where houses lack proper sanitation systems, and (ii) synthetic fertilizers used in agriculture. Similar behaviour is shown in the Neogene basin of the coastal aquifer of Bou Areg (Re et al., 2013).

4.4.2. Ionic deviation versus conservative freshwater (FW)/seawater mixture (SWmix)

To understand the hydrogeochemical processes that occur in the

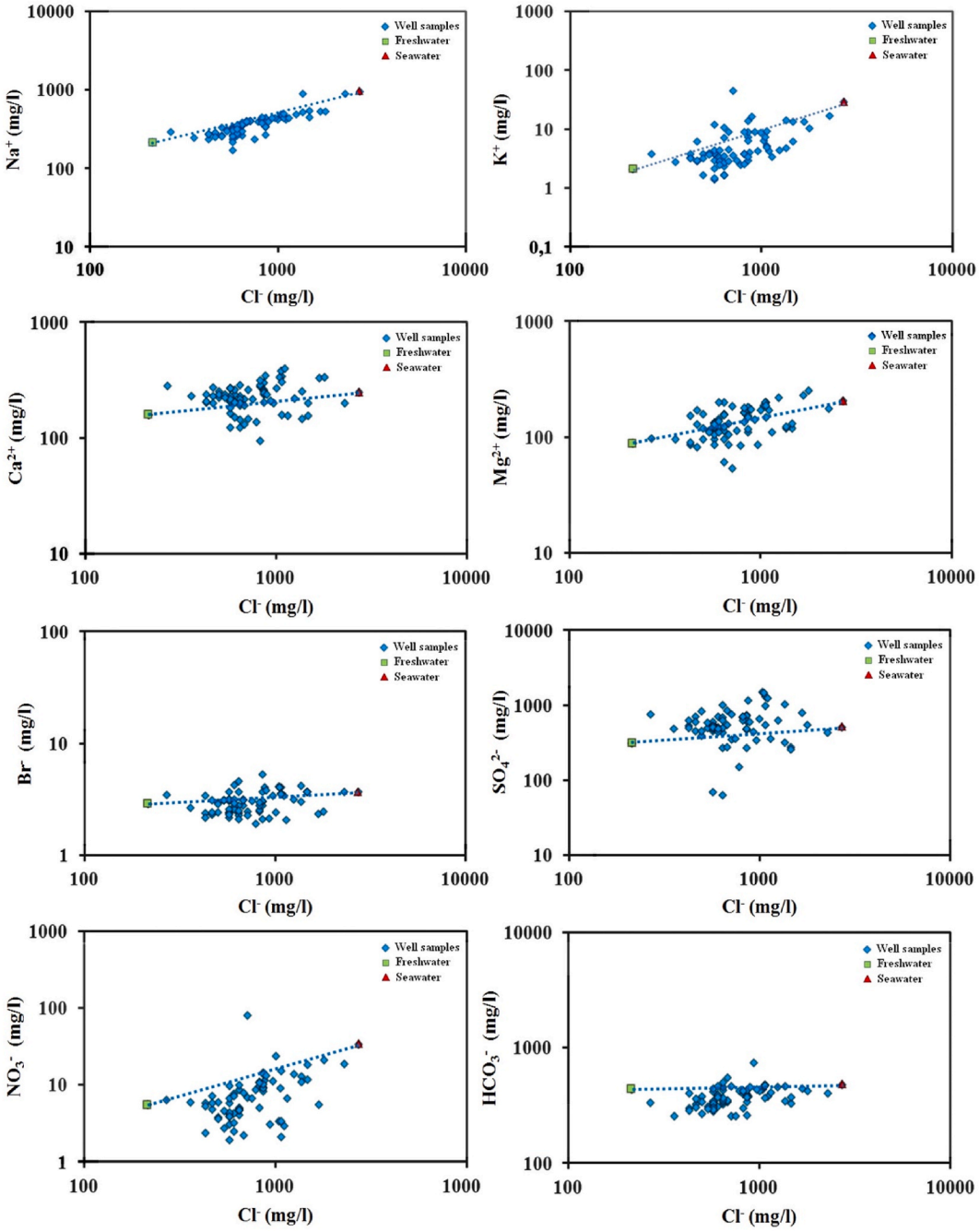

Fig. 10. The Plot of chemical parameters versus Cl^-

aquifer. SI and ionic deviations were determined. The ionic deviations (D) are calculated by comparing each constituent's measured concentration to its theoretical concentration in an established theoretical freshwater–seawater mixture determined from the sample's Cl concentration.

$$\Delta C_i = C_{i,\ simple} - C_{imix} \quad (1)$$

In which ΔC_i denotes the ionic deviation of the ion i, $C_{i,\ sample}$ is the determined ion i concentration in the sample, where $C_{i\ mix}$ is the theoretical ion i concentration for a theoretical (conservative) freshwater–seawater mixture. Depending on the chloride values in the sample ($C_{Cl,\ sample}$), the freshwater Cl concentration ($C_{Cl,f}$), and the saltwater Cl ($C_{Cl,\ sea}$) concentration, the theoretical mixture concentrations were determined, considering the seawater contribution (f_{sea}).

The aquifer water concentration is obtained using the percentage of seawater (fsw).

$$f\text{sea} = \frac{m_{Cl,sample}^{-} - m_{Cl\ ,freshwater}^{-}}{m_{Cl\ ,seawater}^{-} - m_{Cl,freshwater}^{-}} \quad (2)$$

The theoretical concentration from each ion was then calculated using this seawater contribution:

$$C_{i\ \ mix} = f_{sea}.C_{i,sea} + (1 - f_{sea}).C_{i,f} \quad (3)$$

Cl is a conservative tracer (Tellam, 1995); thus, these measurements get it. Because of its high solubility, Cl is seldom eliminated from the system (Appelo and Postma, 1993). To investigate potential mixing with seawater, (Fig. 10) correlates major elements with Cl ions, which can identify the source of salinity and function as a tracer for mixing (Ako et al., 2011; Re et al., 2013; Xing et al., 2013).

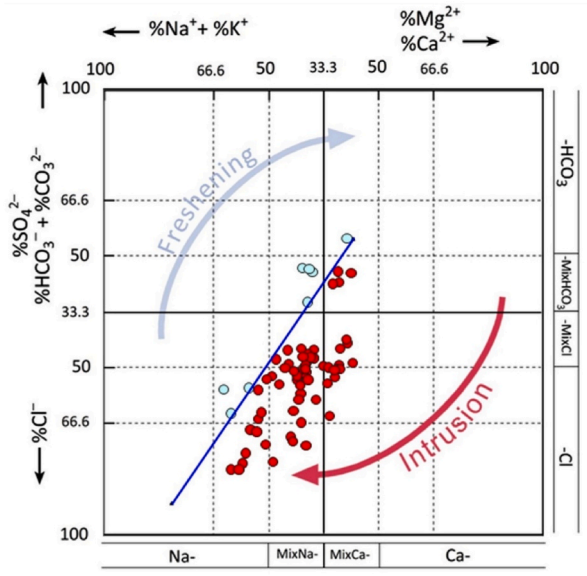

Fig. 11. Representation of Ghiss-Nekkor coastal groundwater samples in the HFE diagram. (modified from (Giménez-Forcada & Sánchez San Román, 2015)).

The excess of Ca for all samples is also clearly observed (Fig. 10). Therefore 76.71% of the sampling points show Ca^{2+} values above the maximum permissible limit according to WHO (200 mg/L). This excess of Ca content has also been observed by other authors (Chafouq et al., 2018) and implicated in various processes, including gypsum and calcite dissolution. Noting also that dissolution of gypsum and evaporation of accumulated water from the Abdelkarim El Khattabi Dam before infiltration plays a significant role in increasing Ca^{2+} in the groundwater of the plain. The ionic relationship between Cl^- and Mg^{2+} (Fig. 10) shows a moderate correlation. In general, higher Ca^{2+} and Mg^{2+} with increasing Cl-values may be attributed to reverse ion exchange (Jankowski et al., 1998) or salt minerals weathering. The dissolution of sedimentary and evaporate rocks that dominate the aquifer of Ghiss-Nekkor is most likely to blame for the high sulfate concentration. Several coastal wells are on the Na–Cl correlation line and are located NE of the plain. This suggests the presence of a freshwater-saltwater mixing mechanism that is not accompanied by ionic exchange processes. Since Cl^- is significantly correlated to Na^+ for most groundwater samples collected in the Ghiss-Nekkor aquifer. They likely come from the dissociation of halite or seawater intrusion. We also note an excess of Na^+ (13, 16, and 22) somewhat related to the dissolution of sodium aluminosilicates than halite which releases one Cl^- for one Na^+.

4.4.3. *Hydrochemical facies evolution diagram*

As per Appelo & Willemsen (1987), the penetration of seawater in a freshwater aquifer triggers the inverse base exchange phenomenon by releasing Ca^{2+} and the fixation of Na^+ by the aquifer matrix. In contrast, Na^+ release and Ca^{2+} fixation (direct base exchange phenomenon) proceed during the refreshing.

Above 71% of the samples are situated in the Mix Na–Cl intrusion zone (Fig. 11). In comparison, more points are localized in the freshening area and achieve the MixNa-HCO_3 and Na–HCO_3 facies. This indicates that the aquifer is ruled by the intrusion phase, caused by an inadequacy of the recharge since the substage has evolved from 5% to 34%. The reversed bases exchange phenomena can describe the formation of the facies Mix Ca–Cl (Fig. 11), induced by seawater intrusion and results in the aquifer matrix fixing Na^+ and liberating Ca^{2+}. This suggestion is corroborated by the existence of the i3 sub-stage (39%) and SW.

5. Conclusions

The present research based on hydrogeochemical parameters combined with statistical analysis showed that local sea intrusion, evaporite dissolution and anthropogenic processes drive groundwater mineralization.

Comparing the data to WHO drinking water standards show that water quality deteriorates. Water sampled in wells 10, 35 and 36 located in the Ajdir (West area), wells 13, 16 and 58 located in the Northeast area (Ahdid), well 65 located near Trougout (East area) and well 22 situated between Beni Bouayach and Imzouren have concentrations above the drinking water law limitations and should thus be treated before to human use. The findings of this research, along with other data on water quality, should be taken into account when formulating plans to ensure that people have safe drinking water. Moreover, the geographical distribution of mineralization revealed that the degradation in groundwater quality was concentrated in the downstream area. Geospatial analysis indicated significant spatial variation and heterogeneity in water quality measurements. In the study area, seawater intrusion is caused by normal faults along the plain to the west and east through which marine waters flow.

Funding

This research work was supported financially by the National Center for Scientific and Technical Research CNRST501100006319 and the Water and Environmental Management team of the Laboratory of Applied Sciences (LSA), National School of Applied Sciences of Al Hoceima.

Declaration of competing interest

The authors declare that they have no known competing financial interests or personal relationships that could have appeared to influence the work reported in this paper.

Acknowledgement

This project was performed as part of the Moroccan MENESFCRS-funded research project PPR2 “Biodiversity and Groundwater Quality in the Al Hoceima Region (Northern Morocco): Application to Hygiene, Monitoring, and Aquifer Protection.” We also thank the anonymous reviewers and the editor for their useful and constructive comments and suggestions that greatly contributed to the improvement of the form and quality of the manuscript.

References

Ako, A.A., Shimada, J., Hosono, T., Ichiyanagi, K., Nkeng, G.E., Fantong, W.Y., Roger, N. N., 2011. Evaluation of groundwater quality and its suitability for drinking, domestic, and agricultural uses in the banana plain (Mbanga, Njombe, Penja) of the Cameroon Volcanic Line. Environ. Geochem. Health 33 (6), 559–575. https://doi.org/10.1007/s10653-010-9371-1.

Alcalá, F.J., Custodio, E., 2008. Using the Cl/Br ratio as a tracer to identify the origin of salinity in aquifers in Spain and Portugal. J. Hydrol. 359 (1–2), 189–207. https://doi.org/10.1016/j.jhydrol.2008.06.028.

Alitane, A., Essahlaoui, A., El Hafyani, M., El Hmaidi, A., El Ouali, A., Kassou, A., El Yousfi, Y., van Griensven, A., Chawanda, C.J., Van Rompaey, A., 2022. Water erosion monitoring and prediction in response to the effects of climate change using RUSLE and SWAT equations: case of R’Dom Watershed in Morocco. Land 11 (1), 93. https://doi.org/10.3390/land11010093.

Appelo, C.A.J., Postma, D., 1993. Geochemistry, Groundwater and Pollution. Balkema, Rotterdam, p. 536.

Appelo, C.A.J., Willemsen, A., 1987. Geochemical calculations and observations on salt water intrusions, I. A combined geochemical/minxing cell model. J. Hydrol. 94, 313–330.

Benabdelouahab, S., Salhi, A., Himi, M., Stitou El Messari, J.E., Casas, A., Mesmoudi, H., Benabdelfadel, A., 2018. Using resistivity methods to characterize the geometry and assess groundwater vulnerability of a Moroccan coastal aquifer. Groundw. Sustain. Dev. 7, 293–304. https://doi.org/10.1016/j.gsd.2018.07.004. July.

Benyoussef, S., El Ouarghi, H., Arabi, M., El Yousfi, Y., Azirar, M., Ait Boughrous, A., 2021. Assessment of the impact of Imzouren city's WWTP on the quality of the surrounding groundwater, at the Rif Central (Northern Morocco). E3S Web of Conferences 240, 1–4. https://doi.org/10.1051/e3sconf/202124001008. April.

Beyene, G., Aberra, D., Fufa, F., 2019. Evaluation of the suitability of groundwater for drinking and irrigation purposes in Jimma Zone of Oromia, Ethiopia. Groundw. Sustain. Dev. 9, 100216 https://doi.org/10.1016/j.gsd.2019.100216. March.

Bieranye, S., Martin, B., Fosu, S.A., Sebiawu, G.E., Jackson, N., Karikari, T., 2016. Assessment of the quality of groundwater for drinking purposes in the Upper West and Northern regions of Ghana. SpringerPlus 1–15. https://doi.org/10.1186/s40064-016-3676-1.

Chafouq, D., El Mandour, A., Elgettafi, M., Himi, M., Chouikri, I., Casas, A., 2018. Hydrochemical and isotopic characterization of groundwater in the Ghis-Nekor plain (northern Morocco). J. Afr. Earth Sci. 139, 1–13. https://doi.org/10.1016/j.jafrearsci.2017.11.007. November.

Connor, R., 2015. The United Nations World Water Development Report 2015: Water for a Sustainable World. UNESCO Publishing, p. 1.

Daniele, L., Vallejos, A., Sola, F., Corbella, M., Pulido-Bosch, A., 2011. Hydrogeochemical processes in the vicinity of a desalination plant (Cabo de Gata, SE Spain). Desalination 277 (1–3), 338–347. https://doi.org/10.1016/j.desal.2011.04.052.

Davis, S.N., Whittemore, D.O., Fabryka-Martin, J., 1998. Uses of chloride/bromide ratios in studies of potable water. Ground Water 36 (2), 338–350. https://doi.org/10.1111/j.1745-6584.1998.tb01099.x.

Dunlop, G., Palanichamy, J., Kokkat, A., EJ, J., Palani, S., 2019. Simulation of saltwater intrusion into coastal aquifer of Nagapattinam in the lower cauvery basin using SEAWAT. Groundw. Sustain. Dev. 8, 294–301. https://doi.org/10.1016/j.gsd.2018.11.014.

Elgettafi, M., Elmandour, A., Himi, M., Casas, A., 2013. The use of environmental markers to identify groundwater salinization sources in a Neogene basin, Kert aquifer case, NE Morocco. Int. J. Environ. Sci. Technol. 10 (4), 719–728. https://doi.org/10.1007/s13762-012-0164-1.

Elmeknassi, M., El Mandour, A., Elgettafi, M., Himi, M., Tijani, R., El Khantouri, F.A., Casas, A., 2021. A GIS-based approach for geospatial modeling of groundwater vulnerability and pollution risk mapping in Bou-Areg and Gareb aquifers, northeastern Morocco. Environ. Sci. Pollut. Control Ser. 28 (37), 51612–51631. https://doi.org/10.1007/s11356-021-14336-0.

Gaaloul, N., Cheng, A.H., 2003. In: Hydrogeological and Hydrochemical Investigation of Coastal Aquifers in Tunisia — Crisis in Overexploitation and Salinization. *Second International Conference on Saltwater Intrusion and Coastal Aquifers*, vol. 13. http://www.olemiss.edu/projects/sciencenet/saltnet/swica2/Gaaloul.pdf.

Gibbs, R.J., 1970. Mechanisms controlling world water chemistry. Science 170 (80), 1088–1090.

Giménez-Forcada, E., 2010. Dynamic of sea water interface using hydrochemical facies evolution diagram. Groundwater 48 (2), 212–216. https://doi.org/10.1111/j.1745-6584.2009.00649.x.

Giménez-Forcada, E., Sánchez San Román, F.J., 2015. An excel macro to plot the HFE-diagram to identify sea water intrusion phases. Groundwater 53, 819–824.

Hamzaoui-Azaza, F., Ketata, M., Bouhlila, R., Gueddari, M., Riberio, L., 2011. Hydrogeochemical characteristics and assessment of drinking water quality in Zeuss-Koutine aquifer, southeastern Tunisia. Environ. Monit. Assess. 174 (1–4), 283–298. https://doi.org/10.1007/s10661-010-1457-9.

Himi, M., Tapias, J., Benabdelouahab, S., Salhi, A., Rivero, L., Elgettafi, M., El Mandour, A., Stitou, J., Casas, A., 2017. Geophysical characterization of saltwater intrusion in a coastal aquifer: the case of Martil-Alila plain (North Morocco). J. Afr. Earth Sci. 126, 136–147. https://doi.org/10.1016/j.jafrearsci.2016.11.011.

Jankowski, J., Shekarforoush, S., Acworth, R.I., 1998. Reverse Ion-Exchange in a Deeply Weathered Porphyritic Dacite Fractured Aquifer System. Water-Rock Interaction, New South Wales, Australia, pp. 243–246. Yass.

Kamal, S., Sefiani, S., Laftouhi, N.E., El Mandour, A., Moustadraf, J., Elgettafi, M., Himi, M., Casas, A., 2021. Hydrochemical and isotopic assessment for characterizing groundwater quality and recharge processes under a semi arid area: case of the Haouz plain aquifer (Central Morocco). J. Afr. Earth Sci. 174, 104077 https://doi.org/10.1016/j.jafrearsci.2020.104077. July.

Kazakis, N., Pavlou, A., Vargemezis, G., Voudouris, K.S., Soulios, G., Pliakas, F., Tsokas, G., 2016. Seawater intrusion mapping using electrical resistivity tomographyand hydrochemical data . An application in the coastal area of eastern Thermaikos Gulf, Greece. Sci. Total Environ. J. 543, 373–387.

Kelly, F., 2005. Seawater Intrusion Topic Paper. Sland Country Health Department.

Kim, J.M., Lee, J., 2017. Time series analysis for evaluating hydrological responses of pore-water pressure to rainfall in a slope. Hydrol. Sci. J. 62 (9), 1412–1421. https://doi.org/10.1080/02626667.2017.1328105.

Kumar, B., 2015. Integrated hydrogeochemical , isotopic and geomorphological depiction of the groundwater salinization in the aquifer system of Delhi, India. J. Asian Earth Sci. https://doi.org/10.1016/j.jseaes.2015.08.018.

Liu, Y., Jiao, J.J., Liang, W., Kuang, X., Table, S., Table, S., Figure, S., 2017. Supplemental Materials for Hydrogeochemical characteristics in coastal groundwater mixing zone. Appl. Geochem. 85, 49–60.

Mahlknecht, J., Merchán, D., Rosner, M., Meixner, A., Ledesma-Ruiz, R., 2017. Assessing seawater intrusion in an arid coastal aquifer under high anthropogenic influence using major constituents, Sr and B isotopes in groundwater. Sci. Total Environ. 587–588, 282–295. https://doi.org/10.1016/j.scitotenv.2017.02.137.

Mohajane, M., Costache, R., Karimi, F., Bao Pham, Q., Essahlaoui, A., Nguyen, H., Laneve, G., Oudija, F., 2021. Application of remote sensing and machine learning algorithms for forest fire mapping in a Mediterranean area. Ecol. Indicat. 129, 107869 https://doi.org/10.1016/j.ecolind.2021.107869. September 2020.

Mondal, N.C., Singh, V.P., Singh, V.S., Saxena, V.K., 2010. Determining the interaction between groundwater and saline water through groundwater major ions chemistry. J. Hydrol. 388 (1–2), 100–111. https://doi.org/10.1016/j.jhydrol.2010.04.032.

Panteleit, B., Kessels, W., Kantor, W., Schulz, H.D., 2001. Geochemical Characteristics of Salinization-Zones in the Coastal Aquifer Test Field (CAT-Field) in North-Germany. First International Conference on Saltwater Intrusion and Coastal Aquifers, p. 11. May 2014.

Piper, A.M., 1944. A graphic procedure in the geochemical interpretation of water-analyses. Eos, Transactions American Geophysical Union 25, 914–928.

Re, V., Sacchi, E., Martin-Bordes, J.L., Aureli, A., El Hamouti, N., Bouchnan, R., Zuppi, G. M., 2013. Processes affecting groundwater quality in arid zones: the case of the Bou-Areg coastal aquifer (North Morocco). Appl. Geochem. 34 (July), 181–198. https://doi.org/10.1016/j.apgeochem.2013.03.011.

Robinove, C.J., Langford, R.H., Brookhart, J.W., 1958. Saline-water resources of North Dakota. US Geological Survey Water Supply 1428, 1–77. http://pubs.er.usgs.gov/publication/wsp1428.

Rochdane, S., Elgettafi, M., El Mandour, A., Himi, M., Casas, A., Daafi, Y., Karroum, M., Chouikri, I., 2022. Contribution of electrical resistivity tomography in the study of aquifer geometry and groundwater salinization of Eastern Haouz and upstream Tassaout domain, Morocco. Environ. Earth Sci. 81 (4), 1–17. https://doi.org/10.1007/s12665-022-10246-7.

Sato, K., Iwasa, Y., 2011. Groundwater Hydraulics. Springer Science & Business Media.

Standard, B., 1997. The Environment Conservation Rules 1997. Government of the People's Republic of Bangladesh, Dhaka.

Tellam, J.H., 1995. Hydrochemistry of the saline groundwaters of the lower Mersey Basin Permo-Triassic sandstone aquifer, UK. J. Hydrol. 165 (1–4), 45–84. https://doi.org/10.1016/0022-1694(94)02583-W.

Trabelsi, R., Abid, K., Zouari, K., 2012. Geochemistry processes of the Djeffara palaeogroundwater (Southeastern Tunisia). Quat. Int. 257, 43–55. https://doi.org/10.1016/j.quaint.2011.10.029.

UNESCO, 2012. World's Groundwater Resources Are Suffering from Poor Governance. UNESCO Natural Sciences Sector News.

Vengosh, A., Pankratov, I., 1998. Chloride/bromide and chloride/fluoride ratios of domestic sewage effluents and associated contaminated ground water. Ground Water 36 (5), 815–824. https://doi.org/10.1111/j.1745-6584.1998.tb02200.x.

WHO, 2011. World Health Organization. Water Quality for Drinking: WHO Guidelines. SpringerReference. https://doi.org/10.1007/978-1-4020-4410-6_184.

WHO, 2017. World Health Organization. Guidelines for Drinking-Water Quality: First Addendum to the Fourth Edition. https://doi.org/10.5005/jp/books/11431_8.

Xing, L., Guo, H., Zhan, Y., 2013. Journal of Asian earth Sciences groundwater hydrochemical characteristics and processes along flow paths in the North China plain. J. Asian Earth Sci. 70–71, 250–264. https://doi.org/10.1016/j.jseaes.2013.03.017.

Yang, Q., Li, Z., Ma, H., Wang, L., Martín, J.D., 2016. Identification of the hydrogeochemical processes and assessment of groundwater quality using classic integrated geochemical methods in the Southeastern part of Ordos basin, China. Environ. Pollut. 218, 879–888. https://doi.org/10.1016/j.envpol.2016.08.017.